Journal of Earthquake Engineering

ISSN: 1363-2469 (Print) 1559-808X (Online) Journal homepage: www.tandfonline.com/journals/ueqe20

Seismic Assessment of a Full-Scale Perimeter-Fixed Ceiling with Hook-And-Loop-Secured Lay-In Tiles Using Shake Table Tests

A. Tiwari , J. Bhatta , R. P. Dhakal , T. J. Sullivan , R. K. Shrestha , M. Rashid , Z. Yan , G.A. MacRae , Jiajun Yu , P. Xiang , Y. Zhang , L. Jia , S. Ramhormozian , G. C. Clifton , P. Quenneville , G. Rodgers & X. Zhao

To cite this article: A. Tiwari , J. Bhatta , R. P. Dhakal , T. J. Sullivan , R. K. Shrestha , M. Rashid , Z. Yan , G.A. MacRae , Jiajun Yu , P. Xiang , Y. Zhang , L. Jia , S. Ramhormozian , G. C. Clifton , P. Quenneville , G. Rodgers & X. Zhao (09 Sep 2026): Seismic Assessment of a Full-Scale Perimeter-Fixed Ceiling with Hook-And-Loop-Secured Lay-In Tiles Using Shake Table Tests, Journal of Earthquake Engineering, DOI: 10.1080/13632469.2026.2710661

To link to this article: https://doi.org/10.1080/13632469.2026.2710661

Published online: 09 Sep 2026.

JOURNAL OF EARTHQUAKE ENGINEERING
https://doi.org/10.1080/13632469.2026.2710661

Seismic Assessment of a Full-Scale Perimeter-Fixed Ceiling with Hook-And-Loop-Secured Lay-In Tiles Using Shake Table Tests

A. Tiwari[a], J. Bhatta[a], R. P. Dhakal[a], T. J. Sullivan[a], R. K. Shrestha[a], M. Rashid[b], Z. Yan[c], G.A. MacRae[a], Jiajun Yu[d], P. Xiang[d], Y. Zhang[a], L. Jia[d], S. Ramhormozian[c], G. C. Clifton[e], P. Quenneville[e], G. Rodgers[f], and X. Zhao[d]

[a]Civil and Environmental Engineering, University of Canterbury, Christchurch, New Zealand; [b]Silvester Clark, Palmerston North, New Zealand; [c]Built Environment Engineering, Auckland University of Technology, Auckland, New Zealand; [d]College of Civil Engineering, Tongji University, Shanghai, China; [e]Civil and Environmental Engineering, University of Auckland, Auckland, New Zealand; [f]Mechanical Engineering, University of Canterbury, Christchurch, New Zealand

ABSTRACT

Grid-and-tile ceiling systems are widely installed in commercial buildings but have frequently experienced damage in past earthquakes, resulting in safety risks, costly repairs, and operational interruptions. The present study examines the seismic performance of a perimeter-fixed ceiling incorporating hook-and-loop-secured lay-in tiles, an improved version of a conventional perimeter-fixed ceiling where tiles are not mechanically fastened to the Tees. Hook-and-loop tape at the tile–Tee interface offers an effective means to prevent tile dislodgement and collapse during shaking. The ceiling was installed over half of the third-floor span of a full-scale, three-storey steel-framed building and subjected to unidirectional and bidirectional excitation as part of the non-structural elements testing program of the New Zealand–China collaborative RObust BUilding SysTem (ROBUST) project. The ceiling was subjected to peak floor accelerations of 1.21 g (vector resultant). The observed median fundamental modal periods and median damping ratios lay in the ranges 0.07–0.08 s and 0.93–2.07%, respectively. The median horizontal acceleration amplification factor was 1.07, and the maximum peak component ceiling acceleration in the vertical direction reached 0.38 g. The maximum displacement recorded in the ceiling was 1.89 mm. Lay-in tiles did not experience any pounding with sprinkler heads, and no ceiling components sustained any damage. The hook-and-loop-secured perimeter-fixed ceiling exhibited improved seismic performance compared with conventional perimeter-fixed ceilings. The use of hook-and-loop tape to mechanically connect lay-in tiles to the Tees was shown to be simple and practical for both new installations and retrofit applications. Overall, the system can be regarded as a low-damage, seismically resilient ceiling solution.

ARTICLE HISTORY
Received 5 March 2026
Accepted 20 July 2026

KEYWORDS
Perimeter-fixed ceiling; lay-in tiles; hook-and-loop tape; shake table; low-damage ceiling; dynamic characterization

1. Introduction

Non-structural elements (NSEs), also known as non-skeletal components, play a significant role in maintaining the functional performance of buildings. Past earthquakes have consistently shown that NSEs are highly vulnerable to damage, frequently leading to substantial economic losses, prolonged operational disruptions, injuries, and, in some cases, fatalities (R. P. Dhakal, Pourali, et al. 2016;

CONTACT A. Tiwari aasish.tiwari@pg.canterbury.ac.nz Civil and Environmental Engineering, University of Canterbury, Private Bag 4800, Christchurch 8140, New Zealand

Miranda et al. 2012; Villaverde 1997). In numerous earthquakes, the extent of NSE damage has exceeded that of the structural system itself (Baird and Ferner 2017; R. P. Dhakal 2010; FEMA-E74, 2012; Sagbas et al. 2024). As noted by Dhakal (2024), the performance of NSEs often dictates overall seismic losses, governing repair and downtime costs under minor to moderate shaking, and significantly contributing to casualties during severe shaking. Furthermore, the construction cost of NSEs (Khakurel et al. 2020; Taghavi and Miranda 2003), coupled with their disproportionate share of earthquake-related losses (Bradley et al. 2009; R. P. Dhakal 2010; O'Reilly et al. 2018), can exceed that of structural components.

Among various NSEs, suspended ceilings, in particular, are prominent NSEs in contemporary structures, concealing mechanical and electrical systems including pipes, ducts, and cable trays within their plenum space while improving visual appeal and acoustic performance. Damage to suspended ceilings in past earthquakes has been extensive, resulting in significant economic losses, interruption to building operation, and casualties (R. P. Dhakal 2010; R. P. Dhakal, MacRae, and Hogg 2011; Motosaka and Mitsuji 2012).

In particular, grid-and-tile ceiling systems are prone to dislodgement of lay-in tiles, which can reduce the in-plane stiffness of the ceiling system, increase deformation demands on the supporting Tees, and potentially initiate progressive failure culminating in ceiling collapse. The present study provides the first experimental investigation of a perimeter-fixed ceiling system with hook-and-loop-secured lay-in tiles, to mitigate tile dislodgement. The present study examines acceleration amplification factors, displacement responses, natural frequencies, and damping ratios of a perimeter-fixed ceiling system with hook-and-loop-secured lay-in tiles. The ceiling was installed over half of the third-floor span of a full-scale, three-storey steel-framed structure and subjected to both unidirectional and bidirectional loadings using shake table tests.

A previous study by the authors investigated the seismic performance of the fully-floating ceiling system installed over the entire Level 2 of the same full-scale test building (Tiwari et al. 2026), whereas the present study investigates the perimeter-fixed ceiling system. Although both studies were conducted using the same experimental facility, testing methodology, and test cases, the fully-floating ceiling system and the perimeter-fixed ceiling system represent two fundamentally different ceiling configurations with different boundary conditions and lateral load-transfer mechanisms, resulting in distinct dynamic characteristics and seismic responses.

2. Background

2.1. Development of Low-Damage Solutions for NSEs

Recent research in earthquake engineering has placed growing emphasis on the development of novel seismic solutions for NSEs, with the aim of reducing damage, lowering repair-related costs, enhancing occupant safety by minimizing the risk of injury or loss of life, and improving the ability of buildings to remain operational after earthquake events (Bhatta and Dhakal 2026; Bhatta et al. 2022; Bianchi et al. 2021; Ditommaso et al. 2025; Jun, Lee, and Bae 2022; Maneetes and Memari 2014; Mulligan, Sullivan, and Dhakal 2022; Pinelli et al. 1996; Pourali et al. 2017; Shrestha et al. 2026; Tiwari et al. 2026; Yagi et al. 2022). These developments have encompassed a range of strategies, including improved restraint detailing, the incorporation of flexible connections to accommodate relative displacements, the incorporation of enhanced energy dissipation mechanisms, and the use of rocking or sliding mechanisms to reduce force transfer to NSEs. Despite these advances, achieving low-damage performance in many commonly used NSE systems remains a challenge.

2.2. Suspended Ceilings

Grid-and-tile and plasterboard suspended ceilings are the two most prevalent types used in practice. In grid-and-tile systems, lay-in tiles are placed within a framework formed by intersecting main-Tees and

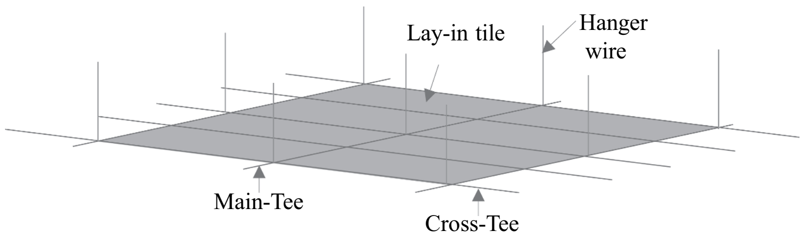

Figure 1. Schematic of the main components of a typical grid-and-tile ceiling system; reproduced from Tiwari et al. (2026).

cross-Tees, typically without mechanical fastening. Plasterboard ceilings, on the other hand, involve securing boards to the underside of furring channels using screws. As a result, the Tees remain visible in grid-and-tile ceilings, whereas the furring channels are hidden in plasterboard ceilings. Figure 1 illustrates the main components of a typical grid-and-tile ceiling system, including the lattice of main-Tees and cross-Tees, the lay-in tiles supported within the lattice, and the hanger wires suspending the ceiling from the floor above.

Grid-and-tile ceiling systems are typically classified according to how lateral forces are transferred to the supporting structure. A brief overview of alternative ceiling systems is first presented to place the perimeter-fixed ceiling investigated in the present study within the broader context of suspended ceiling systems. Perimeter-fixed ceiling systems transfer these forces to the walls (Figs. 2, 3, and 4), whereas braced ceiling systems transfer them to the floor above through braces (Fig. 5). A combination of both systems is also employed, in which the ceiling is fixed to the walls at the perimeter and additionally supported by braces connected to the floor above. Another approach was proposed by Pourali et al. (2017) in the form of a low-damage ceiling concept, termed a fully-floating ceiling system, which is neither attached to the surrounding wall, as in perimeter-fixed ceiling systems, nor supported by braces, as in braced ceiling systems. In the fully-floating ceiling system, the displacement of the freely suspended ceiling is controlled by compressible foam material provided between the ceiling edge and the wall (Fig. 6).

A typical perimeter-fixed ceiling system may have either all four edges fixed (Figs. 2 and 4a) or only two adjacent edges fixed (Figs. 3 and 4). Perimeter-fixed ceilings with all edges fixed are vulnerable to damage caused by differential building movement when the tees are rigidly connected at both ends; consequently, configurations with only two adjacent edges fixed have been promoted in recent years (USG-Boral 2015). Accordingly, the present study investigates a perimeter-fixed ceiling with only two adjacent edges fixed.

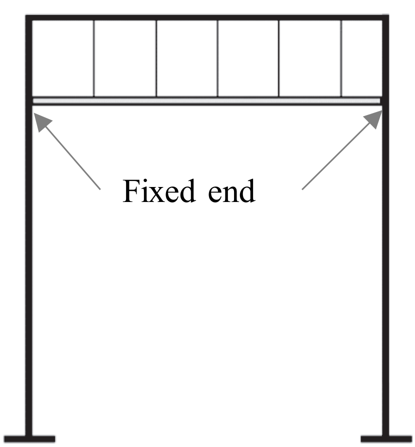

Figure 2. Perimeter-fixed ceiling with four edges fixed; adapted from Pourali (2017).

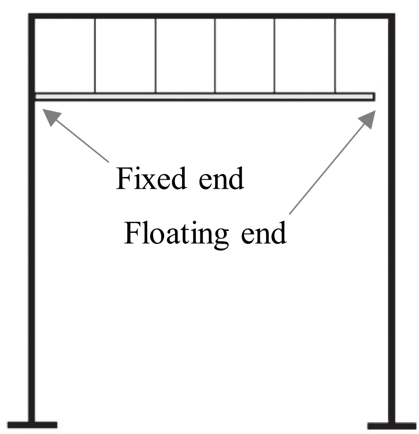

Figure 3. Perimeter-fixed ceiling with adjacent edges fixed; reproduced from Tiwari et al. (2026).

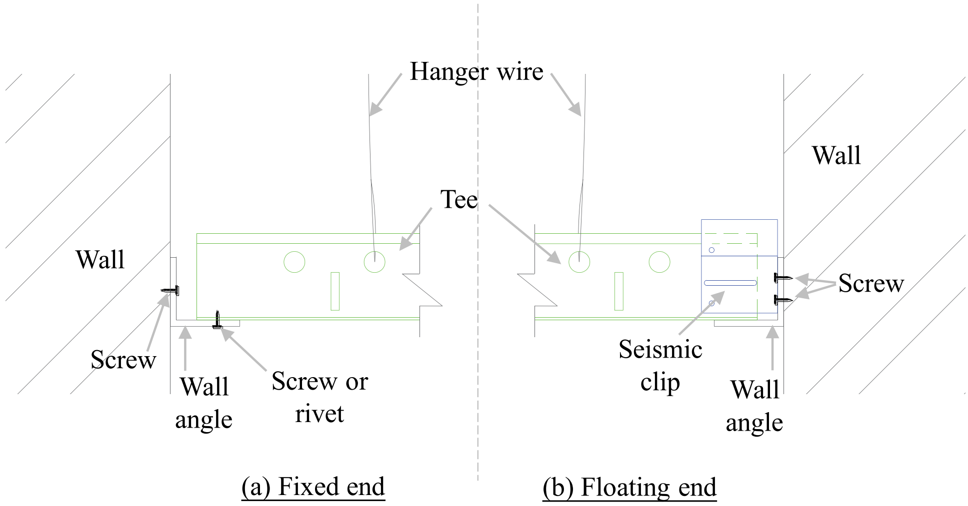

Figure 4. Typical connections between a perimeter-fixed ceiling and the wall.

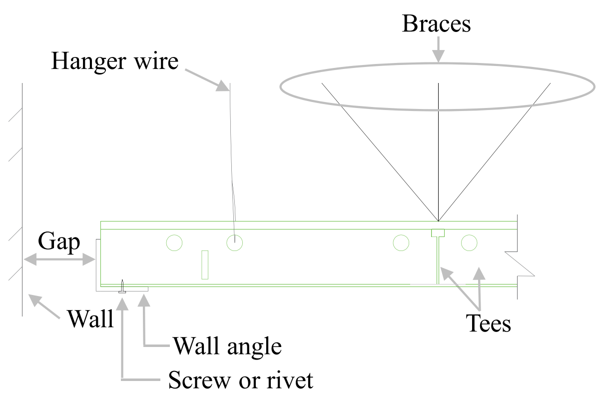

Figure 5. Typical edge details of a braced ceiling at the ceiling-to-wall boundary.

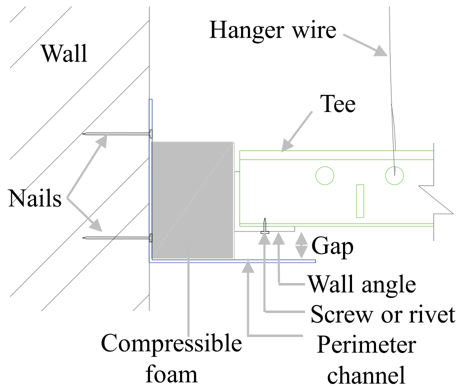

Figure 6. Typical connection details between a fully-floating ceiling and the wall.

In a perimeter-fixed ceiling with only two adjacent edges fixed, the ends of Tees are fixed to wall angles on two adjacent sides of the perimeter using rivets or screws (Fig. 4a), while the ends of Tees on the remaining two sides rest on the wall angles with or without seismic clips (Fig. 4b). Seismic clips allow the Tees to float along their slots. The major demand in this system is the axial force developed along the Tees at the fixed ends connected to the wall angles, which is resisted by the rivets or screws. These forces are then transferred to the wall angles, which are secured to the walls.

2.3. Performance in Past Earthquakes and Previous Studies

Past earthquakes have documented multiple failure mechanisms in perimeter-fixed grid-and-tile ceilings, including main-Tee/cross-Tee intersection failures, Tee compression, buckling and torsion, Tee-wall angle connection detachment, main-Tee splice separations, tile fallout, and tile-sprinkler impacts (Dhakal et al. 2011, Dhakal et al. 2016; Gilani et al. 2010).

Standards such as ASTM-International (2017) specify that ceilings with an area less than 92.9 m^2 may be installed without braces. Limited research has been conducted on perimeter-fixed grid-and-tile ceilings without braces, including studies by Dhakal et al. (2016); Pourali (2017); Ryu and Reinhorn (2019); Soroushian et al. (2019), which have provided invaluable contributions to the field. Despite these works, studies specifically focusing on the prevention of dislodgement of lay-in tiles in such ceilings remain limited.

2.4. Proposed Approach to Prevent Lay-In Tile Dislodgement

FEMA356 (2000) allows the dislodgement of an individual lay-in tile to achieve the Operational Performance Level. Nevertheless, such tile fallout compromises the ceiling's in-plane rigidity, which amplifies Tees deflections and may trigger progressive failures, including additional tile dislodgement and Tee buckling in a cascading manner, as observed by Ryu and Reinhorn (2019) and discussed by Browne, Long, and Stanway (2024). Dislodged tiles may also damage underlying equipment, create perceptions of severe structural distress that induce occupant panic, and lead to full ceiling system collapse, obstructing egress during emergency evacuation and posing direct life-safety hazards. Therefore, preventing the dislodgement of lay-in tiles is essential for maintaining the operational performance of ceiling systems.

Badillo-Almaraz, Whittaker, and Reinhorn (2007) examined retainer clips to prevent lay-in tile dislodgement through dynamic testing of full-scale suspended ceilings. While these clips reduced tile collapse, they increased inertial demands on the Tees, causing damage at lower shaking levels, and complicate access to the plenum space for maintenance of services (Browne, Long, and Stanway 2024; Long et al. 2023). To overcome these limitations, the present study adopts mechanical fastening of lay-in tiles to Tees using hook-and-loop tape. Hook-and-loop tape features a hooked surface paired with a soft loop fabric (Fig. 7), which forms a mechanical bond that can be repeatedly fastened and released (Velcro-Brand n.d.-b). Mechanically connecting tiles with hook-and-loop tape along the Tees' seatings (Fig. 8) is anticipated to minimize dislodgement, enhance in-plane stiffness, and improve the seismic performance of the ceiling system. Tiles secured in this way are hereafter referred to as hook-and-loop-secured lay-in tiles.

2.5. Scope and Limitations of the Study

The present study focuses on the seismic performance of an unbraced perimeter-fixed grid-and-tile ceiling system, in which only two adjacent edges were fixed, and the lay-in tiles were secured using hook-and-loop tape. For brevity, this system is hereafter referred to as a perimeter-fixed ceiling system.

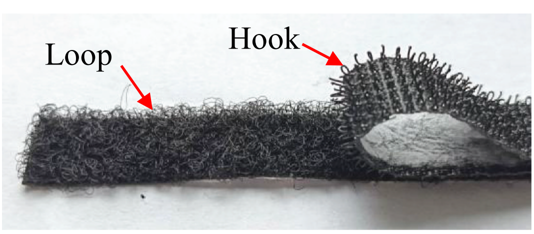

Figure 7. Hook-and-loop tape; reproduced from Tiwari et al. (2026).

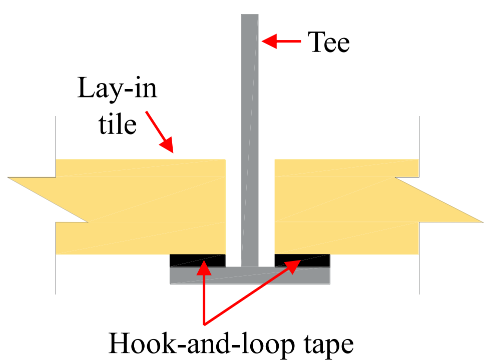

Figure 8. Schematic illustrating the application of hook-and-loop tape between the Tee seatings and the lay-in tiles.

Previous studies have shown that some NSEs, including infill walls, can affect the dynamic response of structures (Ditommaso, Lamarucciola, and Ponzo 2024; Su et al. 2005). However, no evidence has been found to indicate that lightweight ceiling systems influence structural response beyond their contribution to the total seismic mass. Accordingly, the effect of the ceiling system on the dynamic response of the supporting structure is not considered in the present study. The influence of other NSEs, including precast concrete panels and glazed curtain walls, on the behavior of structures is also being examined within the same ROBUST project (Hashemi 2026, PhD Thesis under preparation). Additionally, changes in structural performance were considered negligible, as the structural system remained intact and no damage was observed throughout the tests (ROBUST-Project 2024).

3. Test Setup and Instrumentation

Full-scale shake table experiments on a three-storey steel-framed structure were conducted as part of the New Zealand–China ROBUST collaborative research program. Testing was carried out at the International Joint Research Laboratory of Earthquake Engineering (ILEE), Jiading Campus, Tongji University, Shanghai, China. The program's main goal was to assess low-damage seismic solutions for structural and non-structural systems (R. P. Dhakal et al. 2020; G. A. MacRae et al. 2020). The low-damage structural system comprised two bays along the longitudinal (NS/X) direction and one bay in the transverse (EW/Y) direction, incorporating interchangeable seismic force-resisting systems, one of which is shown in Figs. 9 and 10. Force-resisting configurations included braced frames (Yan et al. 2025), moment frames (Yan et al. 2023), rocking columns (Xie et al. 2021), or rocking frames (Zhang et al. 2026). The floor system comprised a composite steel floor deck using profiled steel sheeting (Steel and Tube 2016). End column centers were spaced at 7250 mm (X-direction), 4750 mm (Y-direction), with 3000 mm storey heights. The building was designed following NZS1170.5 (2016) with a zone factor of 0.40 to represent a typical office structure located in Wellington, New Zealand. Multiple NSEs, including partition walls, glazed curtain walls, precast concrete panels, contents, fire sprinkler piping systems, and suspended ceilings, were evaluated during the last testing sequence of the ROBUST project test series, hereafter termed as NSEs Test for simplicity.

3.1. Structural System for NSEs Test

During the NSEs Test, the longitudinal (NS/X) direction featured a moment resisting steel frame (MRSF) with optimized sliding hinge joints (OSHJs) at the beam-to-column connections. Bay 2 incorporated OSHJs (shown in Fig. 9), whereas Bay 1 used pinned connections. In the transverse (EW/Y) direction, concentrically braced frames (CBFs) with V-bracing were employed, as depicted in Fig. 10. The brace-to-gusset plate connections comprised symmetric friction connections (SFCs) utilizing partially deflected Belleville Springs. Further details of the structural configuration are mentioned in G. MacRae et al. (2024); Yan et al. (2023), and Yan et al. (2024).

To monitor the structural system's response, a combination of accelerometers and string-potentiometers was deployed to measure accelerations and displacements, respectively. At the ground floor and Levels 1 through 3, two accelerometers captured horizontal acceleration along the longitudinal (NS/X) direction, and two accelerometers captured horizontal acceleration along the transverse (EW/Y) direction. Vertical (Z-direction) accelerations were measured using a single accelerometer positioned at the center of each floor slab on Levels 1, 2, and 3. Displacement measurements in both X and Y directions were obtained using two string-potentiometers per floor. Figure 11 presents the instrumentation layout at Level 3, from which the perimeter-fixed ceiling was suspended.

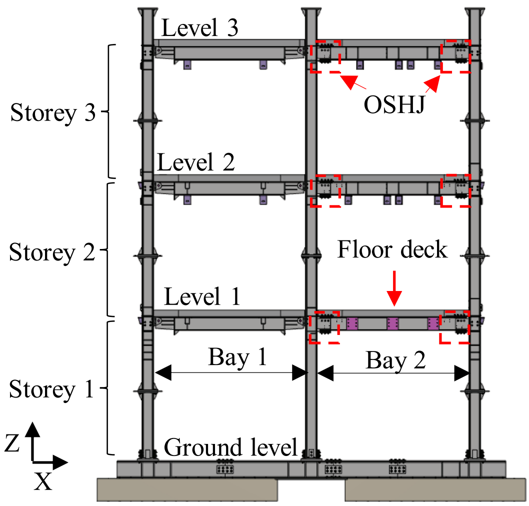

Figure 9. Schematic longitudinal (NS/ X) view of the steel test structure; reproduced from Tiwari et al. (2026).

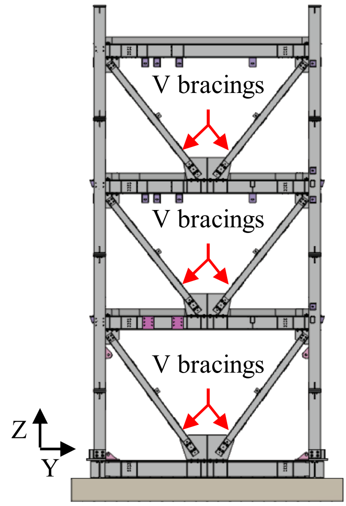

Figure 10. Schematic transverse (EW/ Y) view of the steel test structure; reproduced from Tiwari et al. (2026).

3.2. Perimeter-Fixed Ceiling System

The perimeter-fixed ceiling, measuring 3285 mm by 4500 mm (shown in Fig. 12) was installed over half of the third-storey span (shown in Figs. 11 and 13). The ceiling was suspended 1200 mm below the floor deck using hanger wires with a diameter of 2.68 mm, arranged in an approximately symmetric

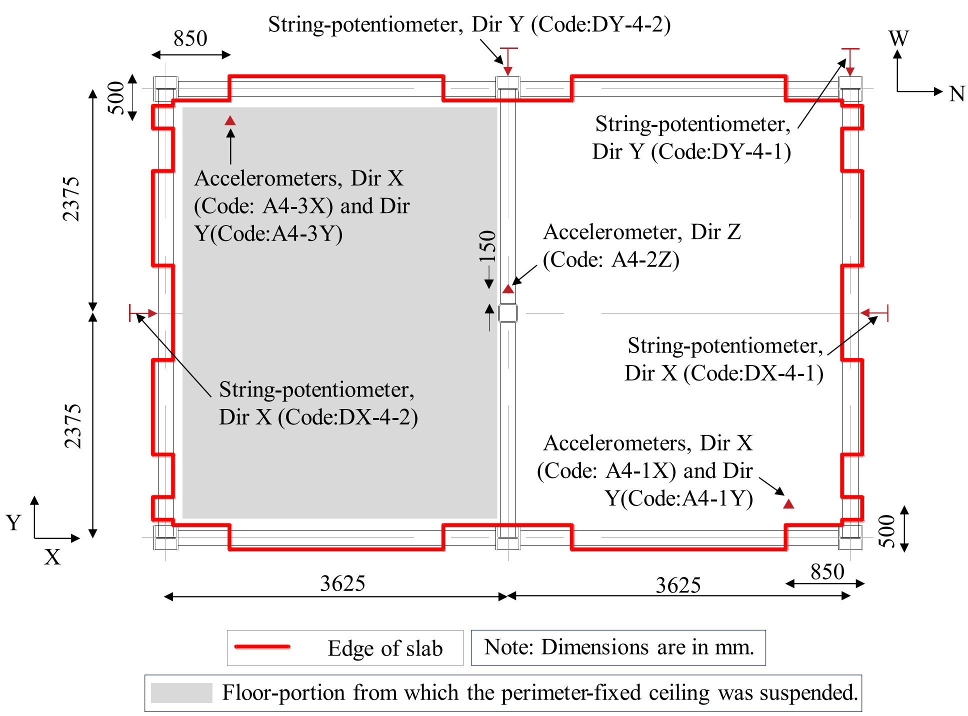

Figure 11. Layout of accelerometers and string-potentiometers on the Level 3 floor.

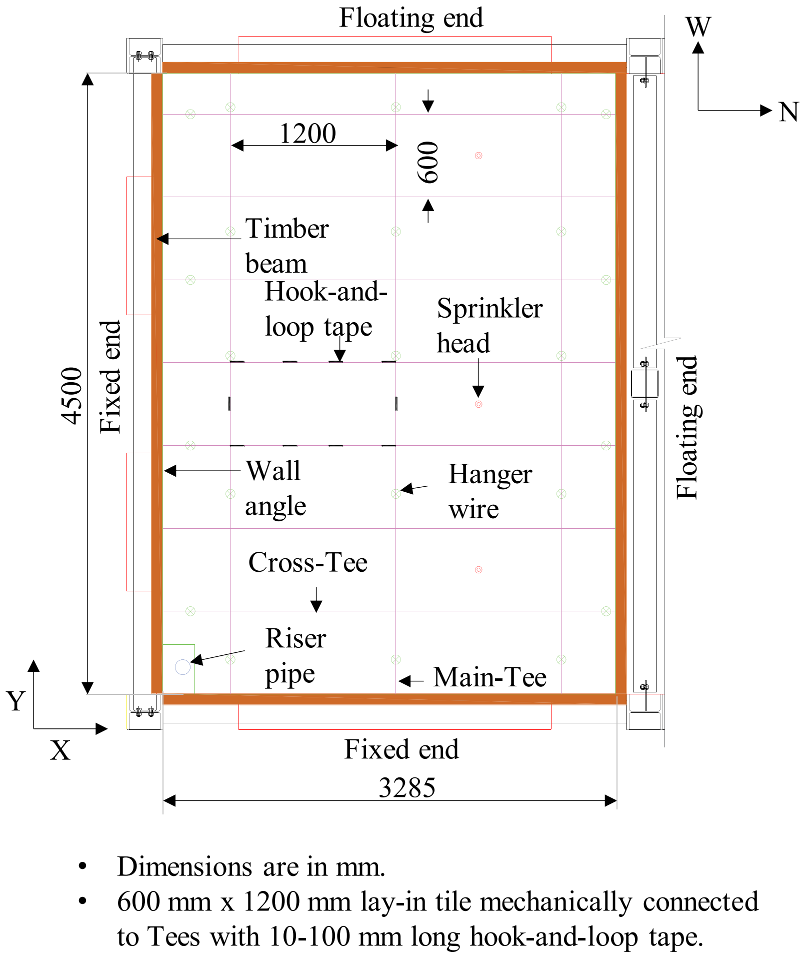

Figure 12. Layout of the tested perimeter-fixed ceiling; adapted from Rashid (2022).

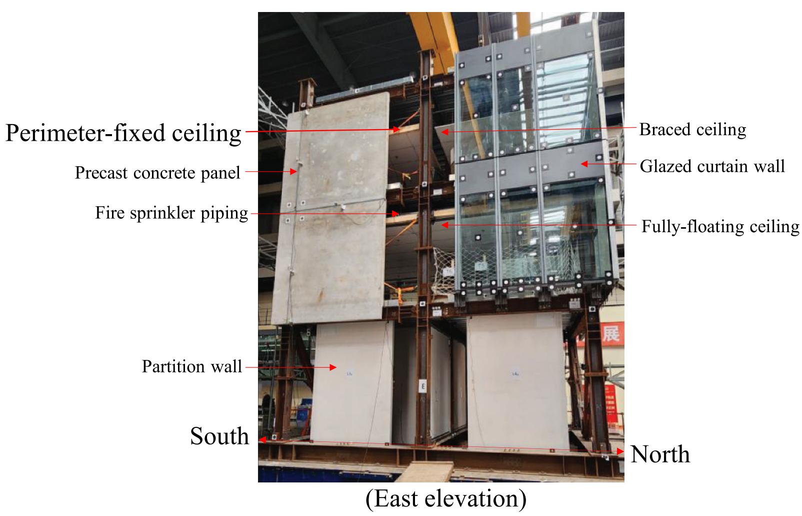

Figure 13. East elevation of the ROBUST test structure with the perimeter-fixed ceiling during NSEs test; adapted from Tiwari et al. (2026).

configuration. Main-Tees along the ceiling's longer dimension were spaced at 1200 mm centers, with cross-Tees connecting them at 600 mm intervals. The Tees at two adjacent ends were fixed to the wall angle using M4 screws of 20 mm in length (these ends are referred as fixed ends). A single M4 screw of Grade 4.6 was deemed sufficient to transfer the axial force predicted at each Tee.

Dhakal et al. (2016) found that perimeter connections become the weakest link (i.e. the first to fail) in perimeter-fixed ceilings with a single rivet connecting the Tees to the wall angles. To prevent early failure in perimeter connections, two screws were used in the present study to secure the ends of the Tees to the wall angles on the two adjacent fixed ends, as shown in Figs. 14 and 15. At the remaining two ends, the Tees rested on the wall angle without attachment and could slide within the slot of the seismic clip affixed to the wall angles, as shown in Fig. 16 (these ends are referred to as floating ends). The wall angles were secured to the timber beams installed between columns.

Typically, ten hook-and-loop tape strips, each measuring 100 mm in length and 10 mm in width (Fig. 17), were used to mechanically connect a 1200 mm by 600 mm lay-in tile to the Tees.

The required amount of hook-and-loop tape was determined by considering both the uplift and horizontal shear demands. The corresponding calculations are summarized in Tables 1 and 2.

For the ceiling system investigated, the uplift mechanism governed the tape requirement, while the shear demand required substantially less tape. This approximate design approach was subsequently validated through shake table tests.

Table 3 summarizes the specifications of the ceiling system components (shown in Fig. 12). Figure 18 provides a brief overview of the installation procedure for the ceiling system. Figures 19 and 20 show the ceiling after completion of installation as viewed from below and in the plenum space, respectively.

In conventional ceiling systems, Soroushian et al. (2012) found that sprinkler heads attached to rigid droppers caused tearing of lay-in tiles, even when 50 mm oversized sleeves were provided. Flexible droppers avoided such damage. Accordingly, flexible droppers were employed in the present study, as they were expected to reduce potential tile damage. Support bars, as shown in Fig. 20, were used to clamp the droppers to the Tees.

Five sensor channels (256 Hz sampling frequency), as shown in Fig. 21, were used to monitor the responses of the ceiling. Three unidirectional accelerometers (A15-X, A15-Y, and A15-Z) were mounted at the geometric center of the ceiling to record acceleration along the three principal

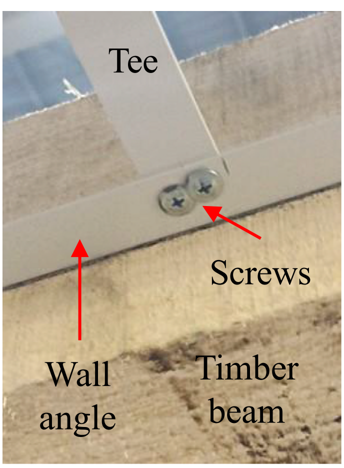

Figure 14. Tee connected to wall angle using double screws at the fixed end.

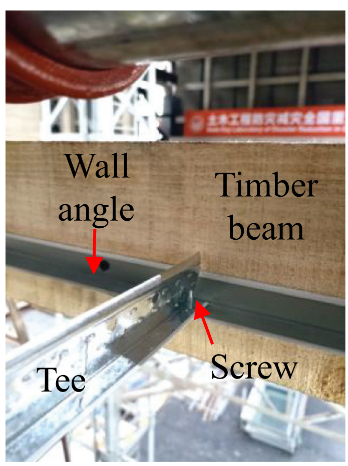

Figure 15. The same connection shown in Fig. 14 as seen from the top.

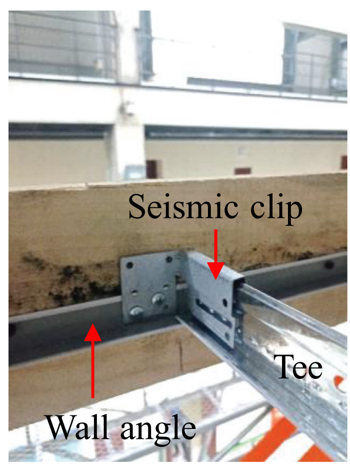

Figure 16. End of Tee inside the slot of seismic clip at the floating end.

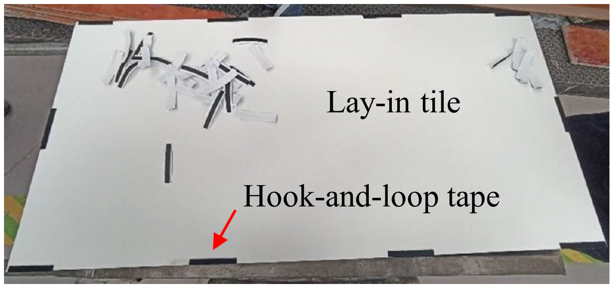

Figure 17. Photograph illustrating the application of hook-and-loop tape to a lay-in tile; adapted from Tiwari et al. (2026).

Table 1. Estimation of required hook-and-loop tape (case: uplift).

Parameter	Symbol	Value	Unit	Remarks
Tile dimensions	–	1200 × 600	mm	Table 3
Tile mass per unit area	–	5.21	kg/m^2	Table 3
Tile mass	m	3.75	kg	
Peak vertical floor acceleration	a_{vf}	0.6	g	Type 2a Structural Test*
Vertical acceleration amplification factor	–	4	–	DZTS1170.5 (2024)#
Peak vertical ceiling acceleration	a_v	2.4	g	
Vertical inertial force	F_v=ma_v	88.32	N	
Peel strength per unit width	p	0.09	N/mm	Manufacturer's datasheet (Velcro-Brand n.d.-a)
Tape width	b	10	mm	
Peel resistance per fastening point	pb	0.9	N	
Required equivalent fastening points	$n \geq F_v/(pb)$	98	–	
Equivalent tape length	–	980	mm	Assuming the smallest practical length of each fastening point to be 10 mm.
Practical number of strips	–	10	–	Detailing requirement†
Tape length per strip	–	98 ≈ 100	mm	
Design outcome	10 strips × 100 mm			

*Approximate vertical floor acceleration under the design-level input (0.4 g PGA) recorded during the Type 2a Structural Test, which was conducted prior to the NSEs Test using the same structural configuration (G. MacRae et al. 2024).
#Draft New Zealand Technical Specification available at the time of testing.
†From a detailing perspective, ten strips were adopted: One near each corner, two along the center of the longer edge, and one along the center of the short edge, as shown in Fig. 17.

Table 2. Estimation of required hook-and-loop tape (case: horizontal shear).

Parameter	Symbol	Value	Unit	Remarks
Peak horizontal floor acceleration	a_{hf}	0.49	g	Type 2a structural Test*
Horizontal acceleration amplification factor	–	4	–	DZTS1170.5 (2024)
Peak horizontal ceiling acceleration	a_h	1.96	g	
Horizontal inertial force	F_h=$m\,a_h$	72.13	N	
Shear strength	–	0.055	N/mm^2	Manufacturer's datasheet (Velcro-Brand, n.d.-a)
Required tape length (10 mm width)	–	132	mm	

*Approximate horizontal floor acceleration under the design-level input (0.4 g PGA) recorded during the Type 2a Structural Test, which was conducted prior to the NSEs Test using the same structural configuration (G. MacRae et al. 2024).

directions, X, Y, and Z. String-potentiometers D23 and D24 were installed to measure the displacement of the floating ends in the Y and X directions, respectively. All sensors were firmly attached to the Tees at their specified locations. Figure 22 shows a representative photograph of accelerometers A15 (A15-X, A15-Y, and A15-Z), and Fig. 23 shows string-potentiometer D23.

Table 3. Typical specifications of components used in the perimeter-fixed ceiling system; reproduced from Tiwari et al. (2026).

Component	Product Name	Material	Dimensions
Main-Tee	Armstrong Peakform Prelude 24 mm	Hot-dipped galvanised steel	24 mm (w) × 43 mm (h) × 3600 mm (l)
Cross-Tee	Armstrong Peakform Cross Tee 1200	Hot-dipped galvanised steel	24 mm (w) × 35 mm (h) × 1200 mm (l)
Wall angle	Armstrong Peakform Wall Angle	Hot-dipped galvanised steel	22 mm (w) × 22 mm (h) × 3000 mm (l)
Tile	Armstrong Ultima Board	Mineral Fibre (5.21 kg/m^2 of 19 mm thick)	1200 mm (l) × 600 mm (w) × 19 mm (t)
Hanger wire	–	Galvanised soft-annealed steel	Diameter of 2.68 mm

w: width; h: height; l: length; t: thickness.

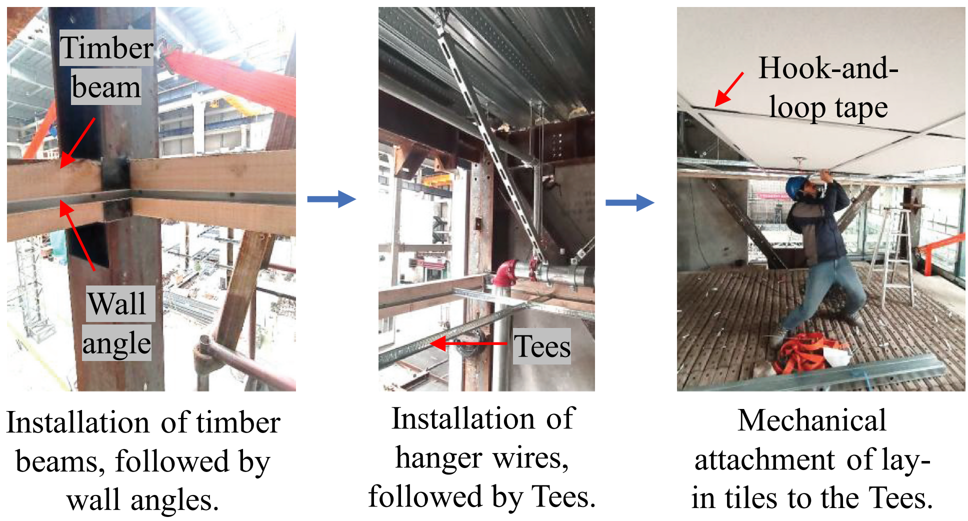

Figure 18. Photographs illustrating the installation of the perimeter-fixed ceiling system.

4. Test Schedule, Data Acquisition, and Signal Processing

The Imperial Valley, El Centro 1940 (Array #9) ground motion was selected and scaled across multiple intensities to match the target response spectrum over the period range of 0.08 s to 1.97 s, which covers all the configurations planned to be tested. The selection criteria and scaling procedure are detailed in Bagheri (2022). During the NSEs Test, the test structure was subjected to a sequence of earthquake excitations with progressively increasing intensity, ranging from the Serviceability Limit State (SLS) up to 1.2 times the Maximum Considered Earthquake (MCE). The structure underwent unidirectional shaking in the X and Y directions separately, as well as bidirectional shaking simultaneously in both directions. Bidirectional white-noise tests (0.05 g) preceded and followed each loading sequence to monitor the dynamic properties of the system.

Ceiling performance was captured via analogue sensors, video recordings, and post-shake inspections (Table 4). Damage documentation included photographs, videos, inspection sheets, and physical measurements. Both the acceleration and displacement records were filtered using a fourth-order low-pass Butterworth filter with a cutoff frequency of 50 Hz.

5. Results and Discussions

This section reports the dynamic characterization results (natural frequencies and damping ratios) and seismic performance metrics of the perimeter-fixed ceiling, including acceleration

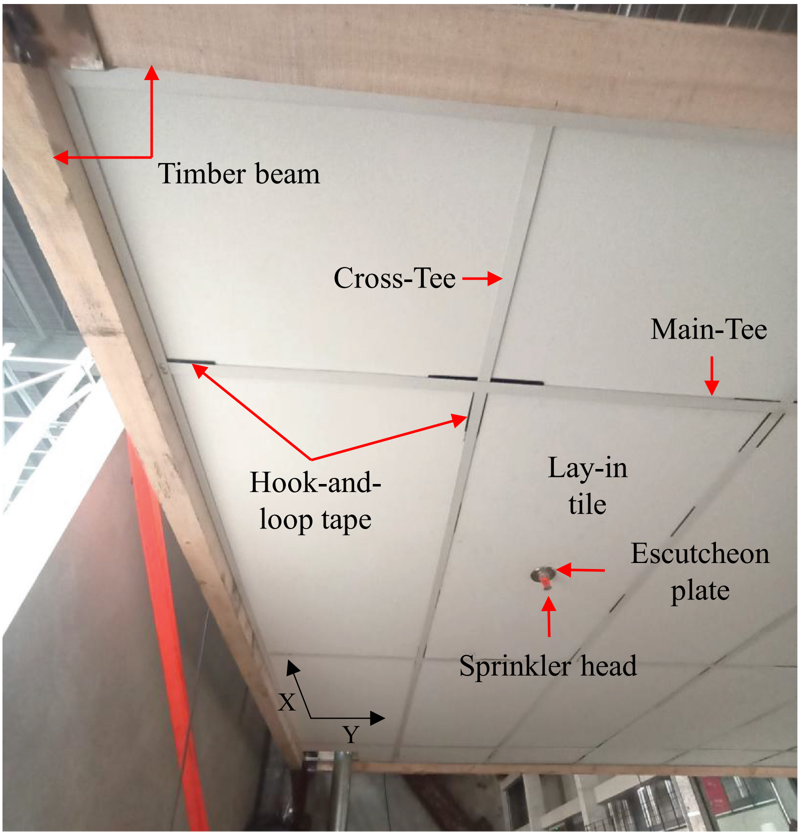

Figure 19. Bottom view of the perimeter-fixed ceiling system.

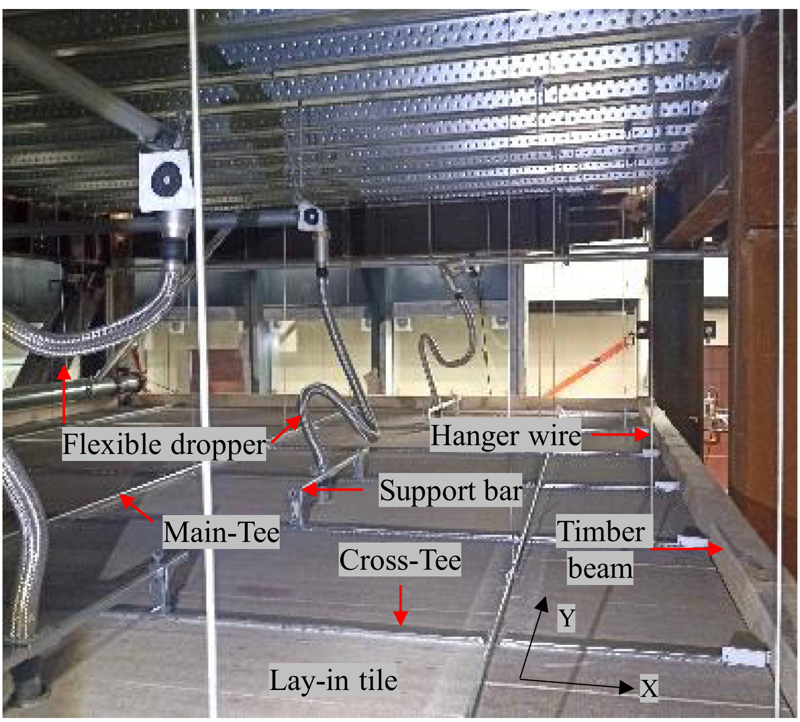

Figure 20. Photograph showing the perimeter-fixed ceiling system within the plenum.

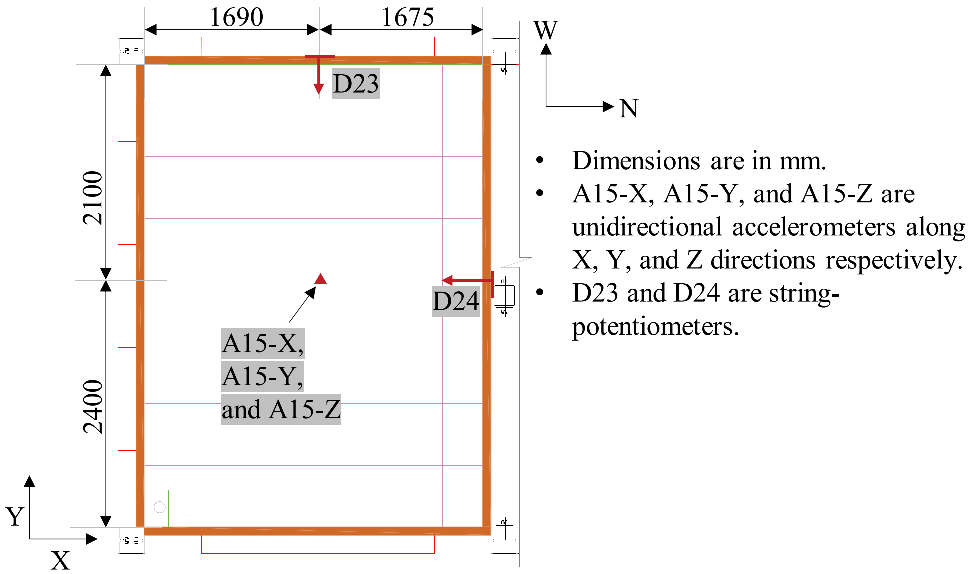

Figure 21. Instrumentation used in the perimeter-fixed ceiling system.

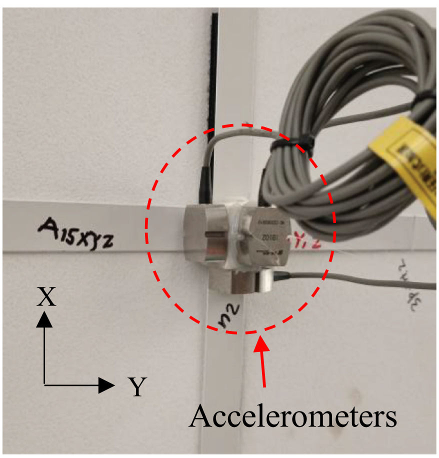

Figure 22. Accelerometers A15 (labelled A15XYZ in the photograph; representing A15-X, A15-Y, and A15-Z).

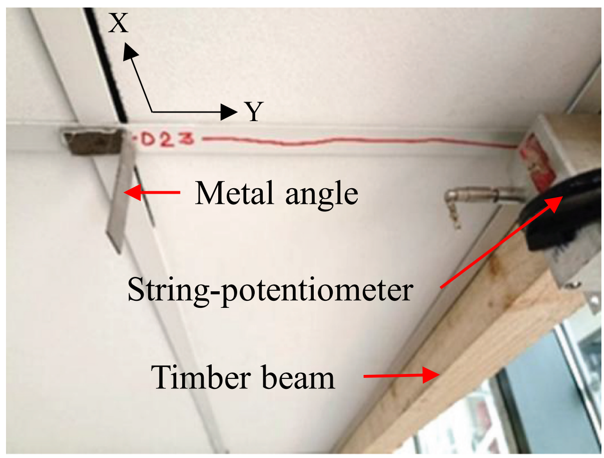

Figure 23. Representative photograph of string-potentiometer D23 measuring displacement in the Y-direction.

amplification factors and displacement responses. The peak floor acceleration (PFA) of the supporting floor is also presented, representing the seismic input demand imposed on the ceiling system.

5.1. PFA Acting on the Perimeter-Fixed Ceiling

During the NSEs Test, ROBUST test structure was subjected to a sequence of progressively increasing unidirectional loading up to 0.6 g in X and Y directions, and bidirectional loading up to 0.88 g in X and Y directions simultaneously (listed in Table 4). When multiple accelerometers were present in a single direction, the average of peak values was taken as the floor PFA in that direction. Figure 24 presents the horizontal PFAs at the Level 3 floor from which the ceiling was

Table 4. Loading sequence applied during the NSEs test phase; adapted from Tiwari et al. (2026).

Test No.	Test case	% MCE	Target Peak Ground Acceleration, g		Remarks
			X	Y	
1	SLS-X	14	0.10	–	
2	SLS-Y	14	–	0.10	
3	SLS-XY1	10	0.07	0.07	
4	SLS-XY2	14	0.10	0.10	Inspection 1
5	2SLS-X	27	0.20	–	
6	2SLS-Y	27	–	0.20	
7	2SLS-XY1	19	0.14	0.14	
8	2SLS-XY2	27	0.20	0.20	Inspection 2
9	3SLS-X	41	0.30	–	
10	3SLS-Y	41	–	0.30	
11	3SLS-XY2	41	0.30	0.30	Inspection 3
12	ULS-X	55	0.40		Inspection 4
13	ULS-Y	55	–	0.40	Inspection 5
14	ULS-XY2	55	0.40	0.40	Inspection 6
15	1.2ULS-X	67	0.49		Inspection 7
16	1.2ULS-Y	67	–	0.49	Inspection 8
17	1.2ULS-XY2	67	0.49	0.49	Inspection 9
18	1.5ULS-X	82	0.60		Inspection 10
19	1.5ULS-Y	82	–	0.60	
20	1.5ULS-XY2	82	0.60	0.60	Inspection 11
21	MCE-XY1	100	0.73	0.73	
22	MCE-XY2	120	0.88	0.88	Inspection 12

SLS: Serviceability Limit State; ULS: Ultimate Limit State; MCE: Maximum Considered Earthquake.

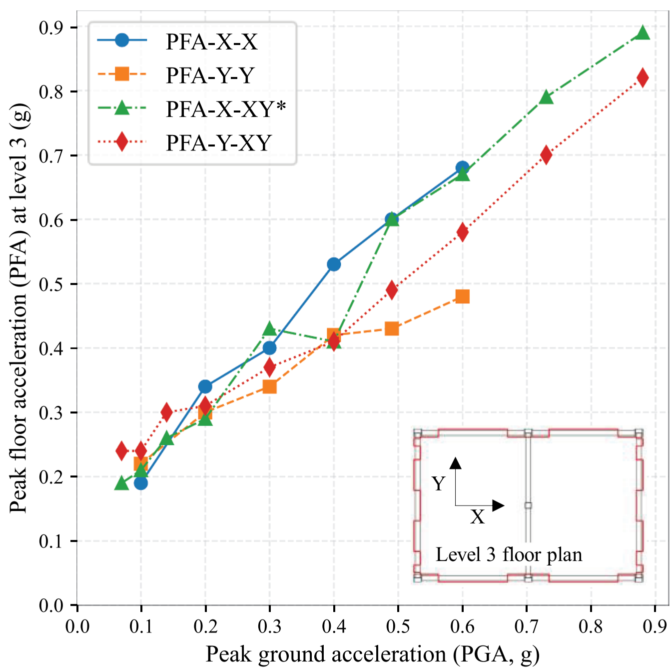

PFA-X-XY*: PFA in X-direction under bidirectional loading in X and Y directions.

Figure 24. Level 3 PFAs of the test structure showing the acceleration demands imposed on the perimeter-fixed ceiling.

suspended. Under bidirectional loading at 0.88 g PGA, the ceiling was subjected to a maximum demand corresponding to a vector resultant horizontal PFA of 1.21 g, comprising 0.89 g in the X-direction and 0.82 g in the Y-direction.

5.2. Natural Frequencies of the Perimeter-Fixed Ceiling

The natural frequencies of the perimeter-fixed ceiling were estimated using acceleration responses induced by 0.05 g bidirectional white noise excitation applied in the X and Y directions. Frequency Response Functions (FRFs) were employed for this purpose and were obtained by normalizing the Fast Fourier Transform (FFT) amplitudes (Arsac 1966) computed from acceleration signals recorded by ceiling-mounted accelerometers (Fig. 21) with the corresponding FFT amplitudes computed from Level 3 floor acceleration signals (Fig. 11). In the X-direction, acceleration signals from the ceiling-mounted accelerometer A15-X (Fig. 21) and the floor-mounted accelerometer A4-3X (Fig. 11) were used to obtain the FRFs. The first dominant peak in each FRF plot was identified, and the corresponding frequency was taken as the ceiling's natural frequency in the X-direction for the corresponding white noise test. Figure 25 illustrates a representative example of identifying the natural frequency from the initial white noise test conducted before the loading tests. For this white noise excitation, the fundamental natural frequency of the ceiling was identified as 13.31 Hz and the corresponding fundamental modal period was 0.08 s. Similarly, the fundamental modal period in the Y-direction was obtained using signals from A15-Y (ceiling-mounted) and A4-3Y (floor-mounted) accelerometers. For the Z-direction, signals from A15-Z (ceiling-mounted) and A4-2Z (floor-mounted) accelerometers were used. Figure 26 presents the range of fundamental modal periods in the X, Y, and Z directions. For the perimeter-fixed ceiling, the median fundamental modal periods were 0.07 s in the X-direction, 0.07 s in the Y-direction, and 0.08 s in the Z-direction.

The next set of unidirectional floor accelerometers in the horizontal directions (A4-1X and A4-1Y, as shown in Fig. 11) was positioned on the opposite corner of the floor, to which the ceiling was not directly attached; however, they were also used to determine the ceiling's fundamental modal period using the same methodology. The median fundamental modal periods obtained from these records were 0.07 s in the X-direction and 0.07 s in the Y-direction. These results matched those obtained from the accelerometers mounted within the floor-portion from which the ceiling was suspended.

The fundamental modal periods in the X and Y directions shown in Fig. 27 (each obtained by averaging the two data sets discussed above) indicate nearly consistent stiffness in their respective

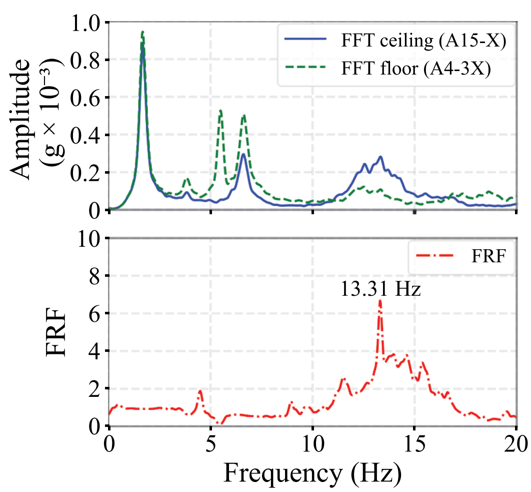

Figure 25. Identified fundamental natural frequency of the perimeter-fixed ceiling system in the X-direction during the initial white noise test carried out prior to the loading tests.

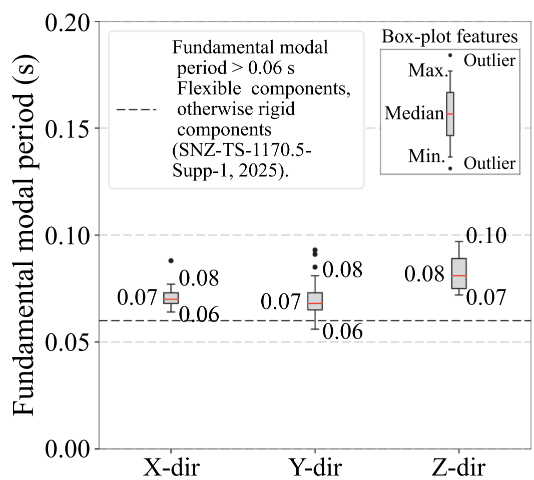

Figure 26. Box-plot showing the range of fundamental modal periods of the perimeter-fixed ceiling system.

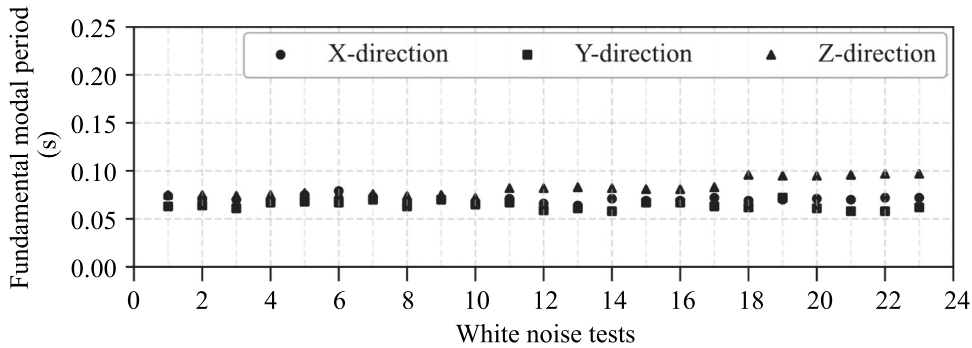

Figure 27. Fundamental modal periods of the perimeter-fixed ceiling system across white noise tests.

directions. In contrast, the modal period in the Z-direction increased by approximately 0.01 s at white noise test 18, which followed the 0.49 g bidirectional loading, suggesting a slight increase in the ceiling's flexibility in the Z-direction.

The Commentary to Structural Design Actions (SNZ-TS-1170.5-Supp-1, 2025) classifies components with a modal period exceeding 0.06 s as flexible. The ceiling investigated in the present study, with a fundamental modal period of 0.07 s, therefore falls within this classification, despite being only marginally above the rigid-component threshold.

5.3. Damping Ratio of the Perimeter-Fixed Ceiling

The FRF plots developed in the earlier section were further utilized to determine the damping ratio of the perimeter-fixed ceiling system using the half-power bandwidth method (Casiano 2016; Clough and Penzien 2003). The lower bandwidth frequency (f_1) and the upper bandwidth frequency (f_2) at either side of the fundamental natural frequency (f_n) were identified. These frequencies (f_1 and f_2) correspond to the 70.7% of the peak amplitude at f_n. The damping ratio, ζ, was then calculated as, $\zeta = (f2 - f1)/(2fn)$. The damping ratio obtained using this method is acceptable for a single-degree-of-freedom system with a damping ratio below 5% (lightly damped system) (Asmussen 1997; Casiano 2016). An example is presented in Fig. 28, showing the damping ratio determination based on the FRF plot shown in Fig. 25.

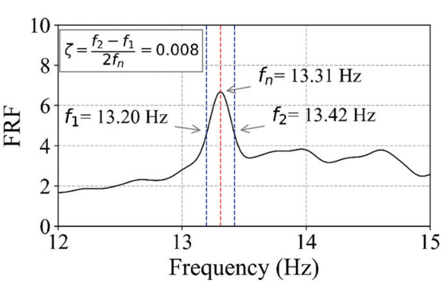

Figure 28. Damping ratio of the perimeter-fixed ceiling system under the first white noise test (half-power bandwidth method).

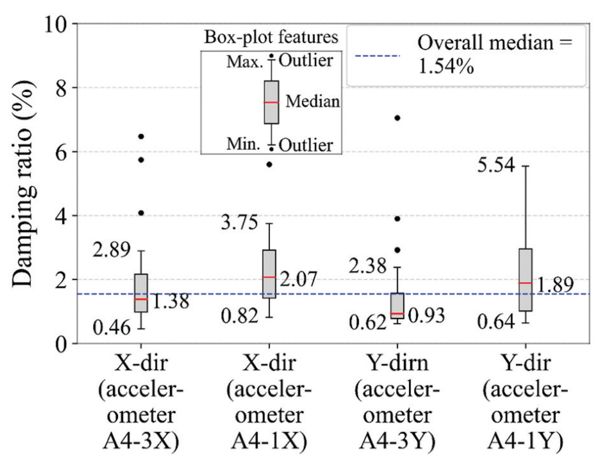

Figure 29. Damping ratio distribution of the perimeter-fixed ceiling system.

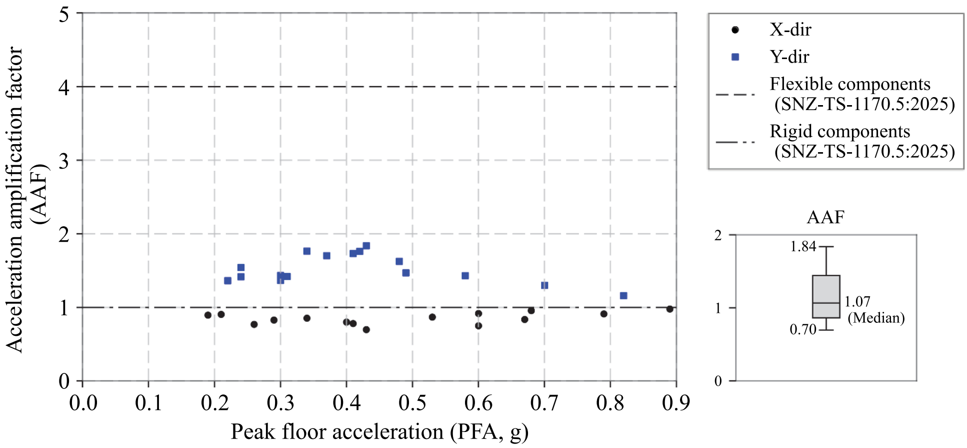

Figure 30. Horizontal acceleration amplification factors of the perimeter-fixed ceiling system.

The estimated median damping ratios shown in Fig. 29 were 1.38% and 2.07% in the X-direction (determined with respect to floor accelerometers A4-3X and A4-1X, respectively), and 0.93% and 1.89% in the Y-direction (determined with respect to floor accelerometers A4-3Y and A4-1Y, respectively). Considering all damping ratio estimates from both directions across the white noise tests, the overall median damping ratio was 1.54%.

5.4. Acceleration in the Perimeter-Fixed Ceiling

5.4.1. Horizontal Acceleration Amplification Factors

For each loading case, the acceleration amplification factor (AAF) of the ceiling was obtained by normalizing the maximum ceiling acceleration by the corresponding maximum floor acceleration. In the X-direction, the AAF was determined using the peak response measured by the ceiling-mounted accelerometer A15-X (Fig. 21) and the corresponding floor acceleration (Fig. 24). An identical procedure was adopted in the Y-direction using acceleration data from the ceiling-mounted accelerometer A15-Y (Fig. 21) and the corresponding floor response (Fig. 24).

The calculated AAFs, presented in Fig. 30 for both unidirectional and bidirectional horizontal excitation (Table 4), varied between 0.70 and 0.98 in the X-direction and between 1.16 and 1.84 in the Y-direction. When results from both directions are considered together, the median AAF is 1.07. These amplification levels remain comfortably below the limiting value of 4 specified by SNZ-TS -1170.5 (2025) for flexible components installed above ground level. The estimated first three modal periods of the structure in the X-direction were 0.67 s, 0.15 s, and 0.08 s, and 0.26 s, 0.07 s, and 0.05 s in the Y-direction (Hashemi 2026, PhD Thesis under preparation). One reason the ceiling experienced higher AAFs in the Y-direction is the occurrence of resonance effects (Haymes, Sullivan, and Hare 2025; SNZ-TS-1170.5-Supp-1 2025), as the fundamental modal period of the ceiling (0.07 s) in the Y-direction coincided with the second modal period of the structure (0.07 s). In contrast, although the ceiling modal period in the X-direction (0.07 s) is close to the third structural modal period (0.08 s), no significant amplification was observed, which may be attributed to the relatively small modal mass participation associated with the third mode.

Pourali (2017) observed AAF of up to 3.5 in perimeter-fixed ceilings with two adjacent ends riveted and remaining adjacent ends floating, similar to those considered in the present study. The high amplification in the study by Pourali (2017) was attributed to lay-in tiles placed on Tees without mechanical connections. In the absence of such restraint, the lay-in tiles slid within the gaps between the lay-in tile and the Tee and, in some cases, impacted the Tees. In contrast, AAF observed in the present study was limited to 1.84. A key distinction lies in the use of hook-and-loop tape in the present study, which restrained the lay-in tiles from sliding within the gaps between the tiles and the Tees, thereby eliminated potential chattering and impact.

5.4.2. Peak Component Ceiling Acceleration in the Vertical Direction

Although the tested building was subjected to only horizontal loadings, the floors also exhibited vertical accelerations, which served as the input for vertical ceiling amplification. In the vertical direction, the peak floor acceleration (PFA-Z) was measured using accelerometer A4-2Z (shown in Fig. 11), while the corresponding peak ceiling acceleration (PCA-Z) was recorded with accelerometer A15-Z (shown in Fig. 21). Both accelerometers were mounted near the geometric center of their respective elements.

As shown in Fig. 31, the PCA-Z varied between 0.03 g and 0.38 g, resulting in amplification factors which are within the code component amplification factor of 4, as specified by SNZ-TS-1170.5 (2025) for flexible components.

Pourali (2017) reported vertical acceleration in perimeter-fixed ceilings reaching values as high as 6 g (amplification factor of 21) under boundary conditions comparable to those considered in the present study. The pronounced amplification in the study by Pourali (2017) was linked to lay-in tiles simply resting on Tees without mechanical connections, allowing the tiles to uplift, strike the supporting Tees, and become partially dislodged, as discussed in a later section.

By contrast, the present study recorded much lower vertical acceleration, limited to 0.38 g (amplification factor of 2.85). While unrestrained ceilings could experience uplift when the upward absolute vertical acceleration exceeds 1 g, the use of hook-and-loop tape effectively prevented tile uplift and reduced the risk of dislodgement. The reported range, 0.03 g to 0.38 g, represents the dynamic vertical acceleration after removal of the static component (gravity). The maximum dynamic vertical acceleration recorded in the upward direction was 0.37 g, i.e. a value within the reported range of 0.03 g to 0.38 g (Fig. 31). This indicates that uplift could have occurred in an unrestrained lay-in tile.

5.5. Peak Ceiling Displacement of the Perimeter-Fixed Ceiling

Peak ceiling displacements (PCD), as shown in Fig. 32, were obtained from string-potentiometers (D24 in the X-direction and D23 in the Y-direction) installed at the floating ends of the ceiling (shown in Fig. 21). The maximum displacement recorded was 1.89 mm at 0.89 g PFA in the X-direction under bidirectional loading of 0.88 g PGA. Overall, displacements in the X-direction tended to be slightly

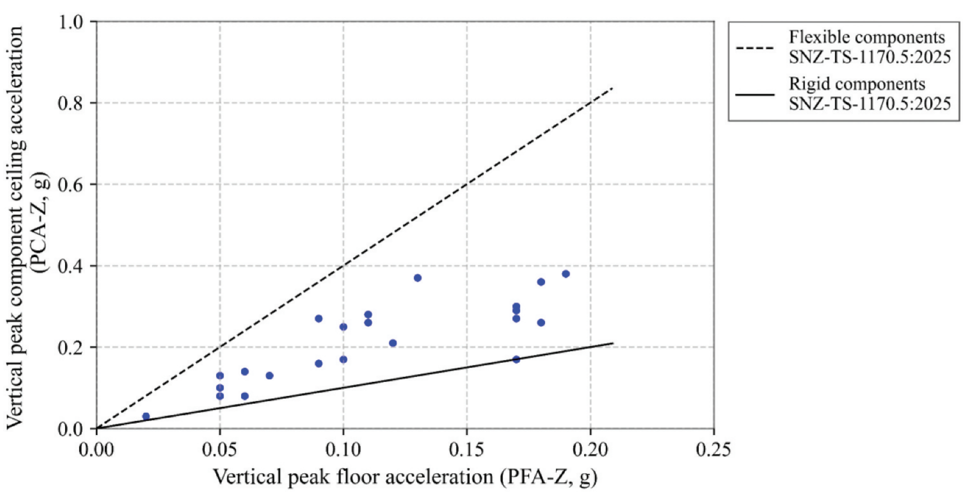

Figure 31. Peak component ceiling acceleration of the perimeter-fixed ceiling in the Z-direction.

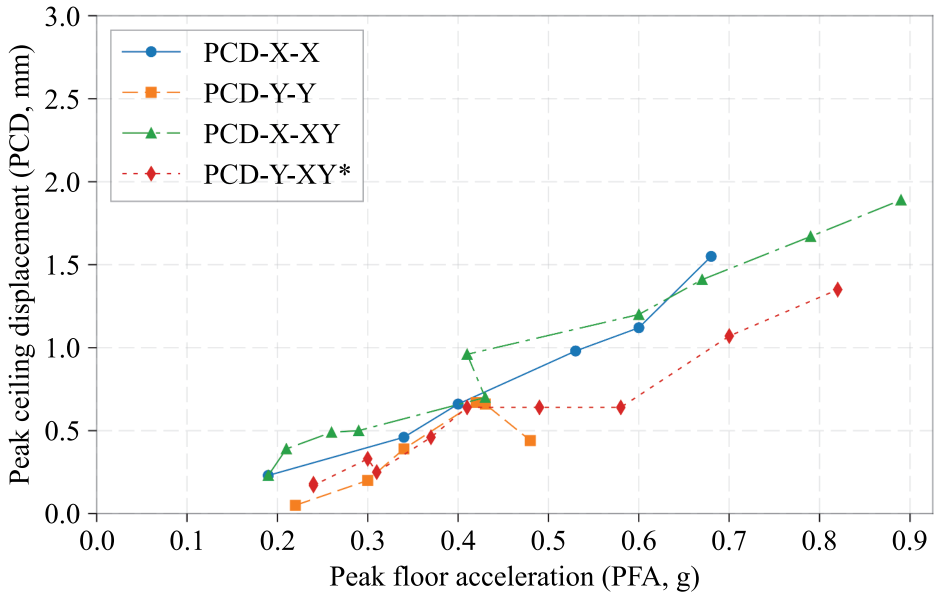

PCD-Y-XY*: PCD in Y-direction under bidirectional loading in X and Y directions.

Figure 32. Peak ceiling displacement of the perimeter-fixed ceiling system.

larger than those in the Y-direction, although the differences were not substantial. This trend is consistent with the variation observed in PFA, as illustrated in Fig. 24. The ceiling displacements were low, as expected for a perimeter-fixed ceiling. For comparison, Pourali (2017) reported a maximum displacement of 2.10 mm for a perimeter-fixed ceiling with similar boundary conditions.

5.6. Force–Acceleration Relationship

The inertial force that gets transferred at the fixed end of the Tee can be predicted by Eq. (1).

$$F = ma \tag{1}$$

Where, “F” is the predicted force at the fixed end of the Tee, “m” is the tributary mass associated with the Tee, and “a” is the peak ceiling acceleration in the direction considered.

For the largest tributary area (shown in Fig. 33), the maximum inertial force of 262.19 N was predicted at the fixed end of the main-Tee (J1 shown in Fig. 34). These forces were calculated by multiplying the tributary mass by the peak ceiling acceleration in the considered direction. The higher inertial force at J1 compared to J2 is attributed to the larger tributary area associated with the main-Tee having fixed end J1, as well as the higher peak ceiling acceleration observed in the Y-direction relative to the X-direction (can be implied from Fig. 30). Pourali (2017) reported that the forces predicted at the fixed ends of the Tees were consistently higher than the measured forces, indicating that this prediction method is conservative.

Based on an ultimate tensile strength of 400 MPa (Grade 4.6), the shear strength of an M4 screw was taken as 240 MPa, resulting in a single-shear capacity of 1685.76 N after applying a partial safety factor of 1.25. Two screws were used for detailing purposes (Dhakal et al. 2016), providing a total shear capacity of 3371.52 N, which is significantly higher than the predicted axial demand of 262.19 N. This quantitative comparison between demand and capacity is consistent with the absence of observed shear damage in the screws.

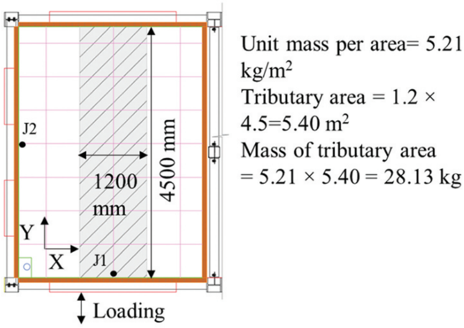

Figure 33. Schematic view of the largest tributary area (hatched) associated with the central main-Tee under loading in the Y-direction.

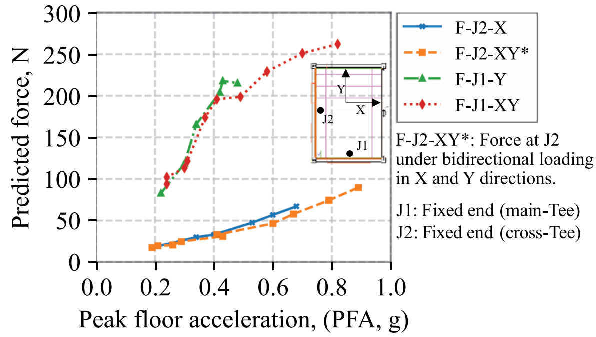

Figure 34. Predicted force at the fixed ends of main-Tee and cross-Tee.

6. Damage Observed in the Perimeter-Fixed Ceiling

During all loading sequences, the perimeter-fixed ceiling remained fully intact, showing no visible signs of damage compared to its condition before testing (shown in Figs. 19 and 20). Typical failure modes, such as dislodgement of lay-in tiles, deformation of Tees, detachment of hanger wires, or damage to wall angles, were not observed in this ceiling system. Sprinkler heads mounted on flexible droppers did not strike the tiles, and clamping the droppers to the Tees with a support bar successfully limited their relative movement, preventing any tearing of the lay-in tiles. To interpret the seismic performance of the tested ceiling and to compare with performance of similar ceilings reported in literature, the damage states defined by FEMA (2003) are used herein (Table 5). The damage states are also related in terms of extent of repairs required.

From Tables 5 and 6, it can be inferred that the ceiling considered in the present study remained below the "Slight" damage state, with no observable damage and no repair action required. Direct quantitative comparison among the ceilings listed in Table 6 is limited mainly due to differences in ceiling dimensions, unit mass, and the experienced PFA. However, the ceiling investigated in the present study is approximately comparable to that studied by Pourali (2017), allowing a qualitative comparison. The hook-and-loop-secured ceiling considered in the present study appears to exhibit improved seismic performance compared with the conventional ceiling studied by Pourali (2017), which did not include mechanical connections of lay-in tiles to the tees. As discussed earlier, another method of securing lay-in tiles is the use of retainer clips. While retainer clips reduce tile collapse, they increase Tee forces, often leading to Tee failures at lower shaking levels (Badillo-Almaraz, Whittaker, and Reinhorn 2007). In contrast, the hook-and-loop-secured lay-in tile ceiling system tested in this study exhibited no damage throughout the test program. This indicates that the procedure adopted to estimate the quantity of hook-and-loop tape provided a conservative basis for the ceiling system investigated in the present study. This suggests that estimating the required quantity of hook-and-loop tape based on the uplift demand may provide a practical basis for similar ceiling systems.

The perimeter-fixed ceiling system investigated in the present study and the fully-floating ceiling system investigated by authors in the previous study (Tiwari et al. 2026) are fundamentally different ceiling systems with different boundary conditions and lateral load-transfer mechanisms. Accordingly, the following discussion is limited to a qualitative comparison of

Table 5. Damage description defined by FEMA (2003).

Damage state	Description of damage	Action
Slight	Few lay-in tiles have dislodged or fallen.	Minor repair works.
Moderate	Excessive falling of lay-in tiles, Tees disconnected or buckled locally.	Moderate repair works.
Extensive	Extensive Tees buckling, local collapse of ceiling at a few locations.	Heavy repair works.
Complete	Global buckling and/or collapse of ceiling system.	Complete replacement.

Table 6. Damage experienced by similar ceiling types in previous studies.

Author	Damage	PFA, g	Length × Width, (m^2)	Mass (kg/ m^2)	Damage state/ Action
(Pourali 2017)	• Partial dislodgement of tiles. • Damaged in the cross-Tee and main-Tee connections. • Tearing in the main-Tee slot. • Bending in cross-Tee clips.	1.50*	4.80 × 2.40	3.80–6.40	Moderate repair works.
(Soroushian et al. 2019)	Unseating of Tee members at floating end. Bending of Tee latches. Lay-in Tile fallout. Tearing of lay-in tiles due to interaction with fire sprinkler piping.	0.54 0.88 1.03 1.40	8.50 × 10	6.12	Moderate repair works.
(Ryu and Reinhorn 2019)	Onset of reparable damage, such as minor dislocations of lay-in tiles or Tees, failure of perimeter components, and failure of Tee connections.	0.61	16.15 × 6.10	6.84	Moderate repair works.
Present study	• No damage.	1.21	4.50 × 3.29	5.21	–

1.5*: Only the maximum PFA was reported; intermediate test PFAs were not available.

their seismic performance. As expected, the perimeter-fixed ceiling system, with its shorter fundamental modal period and smaller ceiling displacements, exhibited as a less flexible system than the fully-floating ceiling system. Importantly, both hook-and-loop-secured ceiling systems remained intact throughout the test program, demonstrating that the hook-and-loop tape solution to prevent tile dislodgement was effective for both ceiling systems.

7. Conclusions

The perimeter-fixed ceiling with hook-and-loop-secured lay-in tiles, an improved version of a conventional perimeter-fixed ceiling (where tiles are not mechanically connected to the Tees), was installed over the half span of third floor of a full-scale, three-storey steel-framed building. The ceiling was subjected to unidirectional and bidirectional loadings during the NSEs Test, the last testing sequence of the NZ-China collaborative ROBUST project test series. Hook-and-loop tape was applied at the interface between the lay-in tiles and the Tees, offering a simple and novel method to prevent tile dislodgement, a failure mode often observed in previous earthquakes. The tested ceiling experienced a maximum peak floor acceleration of 0.89 g in the X-direction and 0.82 g in the Y-direction, with an equivalent vector resultant of 1.21 g, under a bidirectional target PGA of 0.88 g. The key findings for the hook-and-loop-secured perimeter-fixed ceiling are summarized below:

(1) Considering the X and Y directions (horizontal) and the Z-direction (vertical), the median fundamental modal periods ranged from 0.07 s to 0.08 s. These values exceed the 0.06 s rigid-component threshold specified in SNZ-TS-1170.5-Supp-1 (2025), thereby classifying the ceiling system as flexible, although only marginally above the rigid-component limit.
(2) The median damping ratio of the ceiling system was observed 1.54%.
(3) The median acceleration amplification factor in the horizontal directions was 1.07, well below within the code recommended value of 4 specified by SNZ-TS-1170.5 (2025) for flexible components installed above ground level. Higher AAFs in the Y-direction were associated with resonance between the ceiling fundamental period and the second structural mode.
(4) The maximum vertical peak ceiling acceleration measured 0.38 g, corresponding to an amplification factor of 2.85, which complies with code SNZ-TS-1170.5 (2025) component amplification factor of 4.
(5) The peak ceiling displacement of the tested ceiling was 1.89 mm, remaining very low, as expected for this type of ceiling system.

(6) Sprinkler heads attached to flexible droppers, clamped to the Tees, did not impact the lay-in tiles during testing, demonstrating that this configuration is compatible with the hook-and-loop-secured perimeter-fixed ceiling system.
(7) The hook-and-loop-secured perimeter-fixed ceiling sustained no damage throughout the test program, demonstrating superior seismic resilience compared to conventional perimeter-fixed ceilings lacking tile-to-Tee mechanical connections. Furthermore, the hook-and-loop tape connection method proved simple, tool-free, and practical for both new construction and retrofitting applications.

In summary, the hook-and-loop-secured perimeter-fixed ceiling demonstrated robust seismic performance under intense shaking, establishing it as a practical, low-damage solution and a promising strategy for enhancing the seismic resilience of both existing and new perimeter-fixed ceiling systems.

Acknowledgments

The work described was conducted as part of a joint NZ-China research programme with the International Laboratories on Earthquake Engineering (ILEE), Tongji University, Shanghai, China and directly with Tongji University, Shanghai, China. Direct NZ funding is kindly provided by the Building Research Association of NZ (BRANZ) under the Building Research Levy, EQC Toka Tū Ake, the HERA Foundation (a charitable trust associated with the Heavy Engineering Research Association), the Building Innovation Partnership, the Tertiary Education Commission funded QuakeCoRE (the NZ ILEE partner through whom the NZ funding is also coordinated), and the University of Auckland (UA). Administrative and personnel support is also provided by Auckland University of Technology (AUT), University of Canterbury, and the NZ Ministry of Business, Innovation and Employment, Endeavour Programme on Sustainable Earthquake Resilient Buildings for a Better Future - PROP-83779-ENDRP-AUT). Donations of materials are provided by ComFlor, Hilti Corporation, Tracklok, Gripple, Lanyon & LeCompte Construction Ltd., and Alutech Doors & Windows Ltd. Expertise has been generously provided by a number of Chinese and NZ industry representatives. The authors gratefully acknowledge this support. We would like to sincerely thank the RObust BUilding SysTem Project team for their support. Opinions expressed are those of the authors alone. This is QuakeCoRE publication number 1123.

Author Contributions

CRediT: **A. Tiwari:** Conceptualization, Data curation, Formal analysis, Investigation, Methodology, Project administration, Resources, Software, Validation, Visualization, Writing – original draft, Writing – review & editing; **J. Bhatta:** Conceptualization, Supervision, Validation, Writing – review & editing; **R. P. Dhakal:** Conceptualization, Funding acquisition, Project administration, Resources, Supervision, Validation, Writing – review & editing; **T. J. Sullivan:** Supervision, Validation, Writing – review & editing; **R. K. Shrestha:** Writing – review & editing; **M. Rashid:** Resources, Writing – review & editing; **Z. Yan:** Project administration, Writing – review & editing; **G.A. MacRae:** Funding acquisition, Project administration; **Jiajun Yu:** Writing – review & editing; **P. Xiang:** Funding acquisition, Project administration; **Y. Zhang:** Writing – review & editing; **L. Jia:** Funding acquisition, Project administration; **S. Ramhormozian:** Funding acquisition, Project administration; **G. C. Clifton:** Funding acquisition, Project administration; **P. Quenneville:** Funding acquisition, Project administration; **G. Rodgers:** Funding acquisition, Project administration; **X. Zhao:** Funding acquisition, Project administration.

Disclosure Statement

No potential conflict of interest was reported by the author(s).

ORCID

R. P. Dhakal http://orcid.org/0000-0001-5524-5919

Data Availability Statement

The data that support the findings of this study are partially available in figshare at https://doi.org/10.6084/m9.figshare.32229678. Due to the ongoing nature of the project, the complete datasets cannot be made publicly available at this stage.

References

Arsac, J. 1966. *Fourier Transforms and the Theory of Distributions*. Englewood Cliffs, N.J.: Prentice-Hall.

Asmussen, J. C. 1997. *Modal Analysis Based on the Random Decrement Technique: Application to Civil Engineering Structures*. Aalborg, Denmark: Department of Building Technology and Structural Engineering, University of Aalborg.

ASTM-International. 2017. *E580/E580M-17: Standard Practice for Installation of Ceiling Suspension Systems for Acoustical Tile and Lay-In Panels in Areas Subject to Earthquake Ground Motions*. USA: ASTM-International.

Badillo-Almaraz, H., A. S. Whittaker, and A. M. Reinhorn. 2007. "Seismic Fragility of Suspended Ceiling Systems." *Earthquake Spectra* 23 (1): 21–40. https://doi.org/10.1193/1.2357626.

Bagheri, H. 2022. "Seismic Performance of a Full-Scale Steel Structure Using Resilient Slip Friction Joints." PhD Dissertation, Auckland, New Zealand: Department of Civil and Environmental Engineering, The University of Auckland. https://hdl.handle.net/2292/60019. pp. 243.

Baird, A., and H. Ferner. 2017. "Damage to Non-Structural Elements in the 2016 Kaikōura Earthquake." *Bulletin of the New Zealand Society for Earthquake Engineering* 50 (2): 187–193. https://doi.org/10.5459/bnzsee.50.2.187-193.

Bhatta, J., and R. P. Dhakal. 2026. "Seismic Response Assessment of 'Rocking' Interior Partition Walls with Dual-Slot Tracks Under Different Construction Details." *Journal of Earthquake Engineering*: 1–25. https://doi.org/10.1080/13632469.2025.2612533.

Bhatta, J., R. P. Dhakal, T. J. Sullivan, and M. Lanyon. 2022. "Low-Damage Rocking Precast Concrete Cladding Panels: Design Approach and Experimental Validation." *Journal of Earthquake Engineering* 26 (9): 4387–4420. https://doi.org/10.1080/13632469.2020.1830201.

Bianchi, S., J. Ciurlanti, D. Perrone, A. Filiatrault, A. C. Costa, P. X. Candeias, A. A. Correia, and S. Pampanin. 2021. "Shake-Table Tests of Innovative Drift Sensitive Nonstructural Elements in a Low-Damage Structural System." *Earthquake Engineering and Structural Dynamics* 50 (9): 2398–2420. https://doi.org/10.1002/eqe.3452.

Bradley, B. A., R. P. Dhakal, M. Cubrinovski, G. A. MacRae, and D. S. Lee. 2009. "Seismic Loss Estimation for Efficient Decision Making." *Bulletin of the New Zealand Society for Earthquake Engineering* 42 (2): 96–110. https://doi.org/10.5459/bnzsee.42.2.96-110.

Browne, M., J. Long, and J. Stanway. 2024. *Recommended Practice for Seismic Restraint Design of Suspended Ceilings*. Wellington, New Zealand: New Zealand Society for Earthquake Engineering. https://repo.nzsee.org.nz/handle/nzsee/2710.

Casiano, M. J. 2016. *Extracting Damping Ratio from Dynamic Data and Numerical Solutions*. Huntsville, Alabama, USA: National Aeronautics and Space Administration (NASA).

Clough, R. W., and J. Penzien. 2003. *Dynamics of Structures*. 3rd ed. Berkeley, USA: Computers & Structures, Inc.

Dhakal, R. 2024. "Seismic Design of Buildings: Where to Next?" *Bulletin of the New Zealand Society for Earthquake Engineering* 57 (1): 1–17. https://doi.org/10.5459/bnzsee.1680.

Dhakal, R. P. 2010. "Damage to Non-Structural Components and Contents in 2010 Darfield Earthquake." *Bulletin of the New Zealand Society for Earthquake Engineering* 43 (4): 404–411. https://doi.org/10.5459/bnzsee.43.4.404-411.

Dhakal, R. P., G. A. MacRae, and K. Hogg. 2011. "Performance of Ceilings in the February 2011 Christchurch Earthquake." *Bulletin of the New Zealand Society for Earthquake Engineering* 44 (4): 377–387. https://doi.org/10.5459/bnzsee.44.4.377-387.

Dhakal, R. P., G. A. Macrae, A. Pourali, and G. Paganotti. 2016. "Seismic Fragility of Suspended Ceiling Systems Used in NZ Based on Component Tests." *Bulletin of the New Zealand Society for Earthquake Engineering* 49 (1): 45–63. https://doi.org/10.5459/bnzsee.49.1.45-63.

Dhakal, R. P., A. Pourali, A. S. Tasligedik, T. Yeow, A. Baird, G. MacRae, S. Pampanin, and A. Palermo 2016. "Seismic Performance of Non-Structural Components and Contents in Buildings: An Overview of NZ Research." *Earthquake Engineering and Engineering Vibration* 15 (1): 1–17. 10.1007/s11803-016-0301-9.

Dhakal, R. P., M. Rashid, J. Bhatta, C. Chen, G. Q. Song, T. J. Sullivan, G. A. Macrae, G. C. Clifton, P. Xiang, and L. J. Jia. 2020. "Shake Table Testing Plan for Multiple Non-Structural Elements and Contents in a Low-Damage Structural Steel Building." In 17th World Conference on Earthquake Engineering, 17WCEE, 1–12. WCEE: Sendai, Japan.

Ditommaso, R., N. Lamarucciola, and F. C. Ponzo. 2024. "Prediction of the Fundamental Period of Infilled RC Framed Structures Considering the Maximum Inter-Story Drift at Different Design Limit States." *Structures* 63:106422. https://doi.org/10.1016/j.istruc.2024.106422.

Ditommaso, R., F. Scozzese, A. Zona, A. Dall'asta, and F. C. Ponzo. 2025. "Shake-Table Tests for Seismic Performance Assessment of Glass-Aluminium Partition Walls with Viscoelastic Dissipative Devices." *Journal of Earthquake Engineering* 30 (1): 334–357. https://doi.org/10.1080/13632469.2025.2525919.

DZTS1170.5. 2024. *New Zealand Technical Specification*. Standards New Zealand. https://consultations.standards.govt.nz/draft-standards/ts1170-5-public-consultation/user_uploads/20240214-ts-1170.5-public-comment-draft.pdf.

FEMA. 2003. *HAZUS-MH MR4: Multi-Hazard Loss Estimation Methodology, Earthquake Model*. Washington, D.C., USA: Federal Emergency Management Agency (FEMA).

FEMA356. 2000. *Prestandard and Commentary for the Seismic Rehabilitation of Buildings*. Federal Emergency Management Agency (FEMA). https://www.nehrp.gov/pdf/fema356.pdf .

FEMA-E74. 2012. *Reducing the Risks of Nonstructural Earthquake Damage-A Practical Guide* (FEMA- E74). Washington, D.C., USA: Federal Emergency Management Agency.

Gilani, Amir S. J., M. Reinhorn Andrei, B. Glasgow, O. Lavan, and H. K. Miyamoto. 2010. "Earthquake Simulator Testing and Seismic Evaluation of Suspended Ceilings." *Journal of Architectural Engineering* 16 (2): 63–73. https://doi.org/10.1061/(ASCE)1076-0431(2010)16:2(63).

Hashemi, G. 2026. *Realistic Seismic Behaviour of Low Damage Friction Sliding System*. Auckland, New Zealand.: Auckland University of Technology (AUT)]. under preparation.

Haymes, K., T. J. Sullivan, and J. Hare. "Recommendations for the Revision of the Approach for Seismic Design of Parts and Components in New Zealand Design Standards." *Bulletin of the New Zealand Society for Earthquake Engineering* 58 (1): 52–72. https://doi.org/10.5459/bnzsee.1661.

Jun, S.-C., C.-H. Lee, and C.-J. Bae. 2022. "Shake Table Testing of Braced and Friction-Added Suspended Ceilings and Associated Numerical Study." *Engineering Structures* 252:113724. https://doi.org/10.1016/j.engstruct.2021.113724.

Khakurel, S., R. P. Dhakal, T. Z. Yeow, and S. K. Saha. 2020. "Performance Group Weighting Factors for Rapid Seismic Loss Estimation of Buildings of Different Usage." *Earthquake Spectra* 36 (3): 1141–1165. https://doi.org/10.1177/8755293019901311.

Long, J., A. Baird, A. Pourali, and W. Y. Kam. 2023. "Seismic Design of Suspended Lightweight Ceilings – what's the Ductility?" In NZSEE 2023 Annual Conference,1–14. New Zealand Society for Earthquake Engineering: Auckland.

MacRae, G. A., X. Zhao, L. Jia, G. C. Clifton, R. Dhakal, P. Xiang, S. Ramhormozian, and G. Rodgers. 2020. "The China-NZ ROBUST Friction Building Shaking Table Testing Overview." In The 17th World Conference on Earthquake Engineering, 1–10. WCEE: Japan. https://ir.canterbury.ac.nz/bitstreams/91612e40-fe1c-4336-bf25-f515416a4686/download.

MacRae, G., L.-J. Jia, Z. Yan, C. Clifton, S. Ramhormozian, R. Dhakal, P. Xiang, G. Rodgers, P. Quenneville, and X. Zhao. 2024. "The ROBUST Steel Building Response." In NZSEE 2024 Annual Conference, 1–14. NZSEE: Wellington, New Zealand. https://repo.nzsee.org.nz/bitstream/handle/nzsee/2675/MacRae5.pdf?sequence=1&isAllowed=y.

Maneetes, H., and A. M. Memari. 2014. "Introduction of an Innovative Cladding Panel System for Multi-Story Buildings." *Buildings* 4 (3): 418–436. https://doi.org/10.3390/buildings4030418.

Miranda, E., G. Mosqueda, R. Retamales, and G. Pekcan. 2012. "Performance of Nonstructural Components During the 27 February 2010 Chile Earthquake." *Earthquake Spectra* 28 (SUPPL.1): S453–S471. https://doi.org/10.1193/1.4000032.

Motosaka, M., and K. Mitsuji. 2012. "Building Damage During the 2011 off the Pacific Coast of Tohoku Earthquake." *Soils and Foundations* 52 (5): 929–944. https://doi.org/10.1016/j.sandf.2012.11.012.

Mulligan, J., T. J. Sullivan, and R. P. Dhakal. 2022. "Experimental Seismic Performance of Partly-Sliding Partition Walls." *Journal of Earthquake Engineering* 26 (3): 1630–1655. https://doi.org/10.1080/13632469.2020.1733139.

NZS1170.5. 2016. *Structural Design Actions, Part 5: Earthquake Actions-New Zealand, NZS 1170.5: 2004*. Standards New Zealand. https://www.standards.govt.nz/shop/NZS-1170-5-SUPP-12004-INCLUDES-AMDT-1.

O'Reilly, G. J., D. Perrone, M. Fox, R. Monteiro, and A. Filiatrault. 2018. "Seismic Assessment and Loss Estimation of Existing School Buildings in Italy." *Engineering Structures* 168:142–162. https://doi.org/10.1016/j.engstruct.2018.04.056.

Pinelli, J. P., C. Moor, J. I. Craig, and B. J. Goodno. 1996. "Testing of Energy Dissipating Cladding Connections." *Earthquake Engineering and Structural Dynamics* 25 (2): 129–147. https://doi.org/10.1002/(SICI)1096-9845(199602)25:2<129::AID-EQE542>3.0.CO;2-0.

Pourali, A. 2017. *Seismic Performance of Suspended Ceilings*. Christchurch, New Zealand: University of Canterbury.

Pourali, A., R. P. Dhakal, G. Macrae, and A. S. Tasligedik. 2017. "Fully Floating Suspended Ceiling System: Experimental Evaluation of Structural Feasibility and Challenges." *Earthquake Spectra* 33 (4): 1627–1654. https://doi.org/10.1193/092916EQS163M.

Rashid, M. 2022. "Seismic Assessment and Design of Fire Sprinkler Piping System." PhD Dissertation, Christchurch, New Zealand: Department of Civil and Natural Resources Engineering, University of Canterbury. https://doi.org/10.26021/12872], pp. 393.

ROBUST-Project. 2024. *ROBUST Project Test Report*. https://www.dropbox.com/scl/fo/js2sgjkipmr6m517u5iss/AByp LbDzBaRA0FUOvskrAMw/Reports/2024_0529_ILEE%20Report%20V2.3%20(submitted%20to%20ILEE).PDF?rlkey=sc8d4zde9ih0a9cii2dm64jnr&e=2&dl=0.

Ryu, K. P., and A. M. Reinhorn. 2019. "Experimental Study of Large Area Suspended Ceilings." *Journal of Earthquake Engineering* 23 (6): 1001–1032. https://doi.org/10.1080/13632469.2017.1342294.

Sagbas, G., R. Sheikhi Garjan, K. Sarikaya, and D. Deniz. 2024. "Field Reconnaissance on Seismic Performance and Functionality of Turkish Industrial Facilities Affected by the 2023 Kahramanmaras Earthquake Sequence." *Bulletin of Earthquake Engineering* 22 (1): 227–254. https://doi.org/10.1007/s10518-023-01741-8.

Shrestha, R. K., J. Bhatta, R. P. Dhakal, T. J. Sullivan, A. Tiwari, Z. Yan, G. A. MacRae, et al. 2026. "Seismic Response of Rocking Precast Concrete Cladding System in a Full-Scale Three-Storey Building." *Journal of Earthquake Engineering*: 1–26. https://doi.org/10.1080/13632469.2026.2677799. for publication.

SNZ-TS-1170.5. 2025. *Standards New Zealand Technical Specification*. Standards New Zealand. https://www.standards.govt.nz/shop/snz-ts-1170-52025.

SNZ-TS-1170.5-Supp-1. 2025. *Standards New Zealand Technical Specification*. https://www.standards.govt.nz/shop/snz-ts-1170-5-supp-12025. Standards New Zealand.

Soroushian, S., E. Rahmanishamsi, C. Jenkins, and E. M. Maragakis. 2019. "Fragility Analysis of Suspended Ceiling Systems in a Full-Scale Experiment." *Journal of Structural Engineering* 145 (4): 04019005 (04019001–04019013). https://doi.org/10.1061/(ASCE)ST.1943-541X.0002273.

Soroushian, S., L. Ryan Keri, M. Maragakis, E. Sato, T. Sasaki, T. Okazaki, L. Tedesco, E. Zaghi Arash, G. Mosqueda, and D. Alvarez. 2012. "Seismic Response of Ceiling/Sprinkler Piping Nonstructural Systems in NEES TIPS/NEES Nonstructural/NIED Collaborative Tests on a Full Scale 5-Story Building." In Structures Congress 2012, 1315–1326. ASCE. https://doi.org/10.1061/9780784412367.118.

Steel & Tube. 2016. *ComFlor®80 Product Guide*. https://steelandtube.co.nz/sites/default/files/catalogues/Comflor80_PG-Dec2016-01.pdf.

Su, R. K. L., A. M. Chandler, M. N. Sheikh, and N. T. K. Lam. 2005. "Influence of Non-Structural Components on Lateral Stiffness of Tall Buildings." *The Structural Design of Tall and Special Buildings* 14 (2): 143–164. https://doi.org/10.1002/tal.266.

Taghavi, S., and M. M. Miranda. 2003. *Response Assessment of Nonstructural Building Elements (2003/05)*. Pacific Earthquake Engineering Research Center.

Tiwari, A., J. Bhatta, R. P. Dhakal, T. J. Sullivan, R. K. Shrestha, Z. Yan, G. A. MacRae, et al. 2026. "Dynamic Characterization and Seismic Performance of a Fully-Floating Ceiling with Velcro-Secured Lay-In Tiles via Shake Table Tests." *Journal of Earthquake Engineering*: 1–23. https://doi.org/10.1080/13632469.2026.2642761.

USG-Boral. 2015. *Generic Seismic Design for Donn® Exposed Grid Suspended Ceilings (Brochure)*. Auckland: USG-Boral. https://isco.com.vn/pdf/chong-dia-chan--usg-boral-generic-seismic-design-9-15_vi_1604552926.pdf.

Velcro-Brand. n.d.-a. *Hook-And-Loop Tapes*. https://docs.rs-online.com/9147/A700000006830020.pdf.

Velcro-Brand. n.d.-b. *Velcro® Brand Heavy-Duty Mounting Tape*. https://www.velcro.com/products/garage-organization/velcro-brand-extreme-outdoor-tape/.

Villaverde, R. 1997. "Seismic Design of Secondary Structures: State of the Art." *Journal of Structural Engineering* 123 (8): 1011–1019. https://doi.org/10.1061/(ASCE)0733-9445(1997)123:8(1011).

Xie, R., Z. Li, P. Xiang, and L.-J. Jia. 2021. "Dynamic Behaviors of Steel Multiple-Rocking-Column Structural System with Rocking Stoppers." *Engineering Structures* 243:112649. https://doi.org/10.1016/j.engstruct.2021.112649.

Yagi, S., A. Teramoto, T. Yeow, T. Seike, K. Kusunoki, and I. Nakamura. 2022. "Validating Resilient Detailing of Japanese Ceilings, Windows, and Wall Tiles Using an E-Defense Shake-Table Test." *Journal of Earthquake Engineering* 26 (16): 8525–8551. https://doi.org/10.1080/13632469.2021.1988764.

Yan, Z., S. Ramhormozian, G. C. Clifton, G. MacRae, G. Rodgers, P. Quenneville, R. Dhakal, P. Xiang, L. J. Jia, and X. Zhao. 2024. "Shake Table Testing of a Low-Damage Steel Frame Building Incorporating Asymmetric and Symmetric Friction Connections." In *Proceedings of the 11th International Conference on Behaviour of Steel Structures in Seismic Areas*, edited by F. M. Mazzolani, V. Piluso, E. Nastri, and A. Formisano, 607–616. Vol. 519. Switzerland: Springer Nature Switzerland. https://doi.org/10.1007/978-3-031-62884-9_53.

Yan, Z., S. Ramhormozian, G. C. Clifton, P. Quenneville, G. A. MacRae, G. Rodgers, R. P. Dhakal, P. Xiang, L. Jia, and X. Zhao. 2025. "Seismic Performance of Concentrically Braced Frame with Friction Sliding Connections: Learning from Subassembly Component Tests, Numerical Simulations and Shake Table Tests." In SESOC Conference, 392–398. Structural Engineering Society of New Zealand (SESOC): Wellington, New Zealand.

Yan, Z., S. Ramhormozian, G. C. Clifton, R. Zhang, P. Xiang, L.-J. Jia, G. A. MacRae, and X. Zhao. 2023. "Numerical Studies on the Seismic Response of a Three-Storey Low-Damage Steel Framed Structure Incorporating Seismic Friction Connections." *Resilient Cities and Structures* 2 (1): 91–102. https://doi.org/10.1016/j.rcns.2023.02.007.

Zhang, Y., G. A. MacRae, G. Rodgers, L. Jia, K. Rangwani, Z. Yan, Z. Luo, et al. 2026. "Shaking Table Behaviour of a Full-Scale Three Storey Steel Rocking Structure with Tension-Only Frictional Dissipators." *Earthquake Engineering and Structural Dynamics* 55 (9): 1769–1787. https://doi.org/10.1002/eqe.70132. for publication.